Simplified experimental and computational fuel rod models for identifying critical heat flux

Cite as: AIP Conference Proceedings **2323**, 040005 (2021); https://doi.org/10.1063/5.0041497
Published Online: 08 March 2021

Bořek Ozom, Richard Matas, and Jan Sedláček

Simplified Experimental and Computational Fuel Rod Models for Identifying Critical Heat Flux

Bořek Ozom[b)], Richard Matas[a)], Jan Sedláček[c)]

New Technology – Research Centre (NTC), University of West Bohemia, Univerzitní 2732/8, 301 00 Plzen, Czech Republic.

[a)]Corresponding author: mata@ntc.zcu.cz
[b)]borekozomgm@gmail.com
[c)]sedlacek@ntc.zcu.cz

Abstract. The prediction of critical heat flux (CHF) phenomenon at atmospheric pressure was carried out using computational fluid dynamics (CFD) methods. Heat transfer experiments of flow boiling will be validated at the University of West Bohemia, where an experimental apparatus is built. The test section consists of one 3000 mm long resistance heated fuel rod imitator (HRI) with an outer diameter of 9.1 mm placed in an annular tube. Several spacer grids are used on the experimental device to hold the heated rod imitator in its position while improving the internal heat transfer. All simulations presented in this paper started with the same inlet conditions, while the heating input gradually increased until the two-phase flow reached a steady state. The successfully predicted CHF happened through a liquid sublayer dryout under very high vapor volume fractions (93+ %) which led to complete thermal isolation of the HRI. Thanks to the results of the CFD simulations, the temperature measuring system on the experimental loop could be optimized.

INTRODUCTION

The main parameter of many industrial cooling systems is how much heat they can transfer away safely without the occurrence of CHF. Critical heat flux is a phenomenon which may occur in two-phase fluid flow at high surface heat fluxes and flow qualities. It leads to a significant local decrease of the surface heat transfer coefficient (HTC), which results in overheating and damage to the system.

The knowledge of heat-transfer mechanisms under various flow regimes is important for defining safety margins. Many experimental devices have been built around the world to examine CHF mechanisms and develop accurate correlations. At University of Wisconsin – Madison, 2 x 2 square rod bundle geometry has been utilized for experiments, and new CHF data under small modular reactor (SMR) conditions were obtained by Duarte [1]. Furthermore this data was used by Zhao et al. at the Nuclear Power Institute of China and five Liquid Sublayer Dryout (LSD) models were assessed to investigate their application range. When compared with LSD predictions, the experimental data showed good agreement for void fractions lower than 0.7 [2]. A simple loop for modeling the cooling processes of a nuclear reactor fuel rod that allows the observation of CHF was constructed by Lavicka [3] at the University of West Bohemia for measurements at atmospheric pressure. Another experimental loop is located at the Brno University of Technology and research measurements are currently being carried out on it for atmospheric and middle pressure conditions [4]. Many other research groups have measured critical heat fluxes on fuel rod models using different conditions, geometries, materials and surfaces or rod models. The work of Park et al. [5] is an example of an investigation into high pressure and high flow conditions, and the works of Chun et al. [6] study a wide range of pressures. The more recent works include the results of measurements performed at low flow and pressure by Haas et al. [7] and by Mayer et al. [8], and at high pressures by Duarte et al. [1].

Future experiments by the author's team will be focused on gathering new LSD data for vapor volume fractions exceeding 0.9. Due to low surface heat fluxes in the experimental loop at the University of West Bohemia, the CHF

19th Conference on Power System Engineering
AIP Conf. Proc. 2323, 040005-1–040005-8; https://doi.org/10.1063/5.0041497
Published by AIP Publishing. 978-0-7354-4067-8/$30.00

crisis occurs only as film dryout. This phenomenon corresponds mostly to conditions found in boiling water reactors (BWR).

Before CHF prediction simulations, an analysis of computational approaches must be performed to assure that the results will be applicable. CFD simulations performed by other authors in various CFD codes are available. Vyskocil and Macek used the multiphase code NEPTUNE_CFD [9, 10], and Salnikova [11] used the code STAR CD (Simcenter STAR-CCM+ now). The newer works published by Zhang [12, 13] used ANSYS FLUENT for CHF predictions in relatively complex 3D models.

Two-phase flow *per se* is very complicated to solve with CFD methods and the occurrence of CHF makes it even more difficult in terms of boundary conditions and the huge temperature gradients at the heated interface. In the experimental loop at the University of West Bohemia the fluid is under atmospheric pressure. This made the numerical simulations even harder to perform due to a very large density difference between the water and vapor phases. The CFD simulations yielded an initial idea of the two-phase flow and heat transfer along the fuel rod imitator. The CFD simulations published in this paper serve as an initial preview of fluid flow and heat transfer processes in the measured process and must be therefore validated and also extended using more complex CFD models.

DESCRIPTION OF THE EXPERIMENTAL DEVICE

The experimental device mentioned above and by Lavicka [3] has been modified for boiling visualization and the examination of the CHF mechanisms. It consists of a water loop and a test section with a heated fuel rod imitator. A diagram of the experimental device is shown in Figure 1. Distilled water is used as the coolant in the circuit. The liquid is pumped with a diaphragm dosing pump and with a variable-speed circulation pump. A new variable-speed gear-pump will be used for better control of the flow-rate in subsequent experiments.

The coolant is pumped from a reservoir and through the ultrasonic flow-meter to the inlet chamber. The inlet and outlet chambers are the main supporting parts of the experimental device, between which the HRI and the glass pipe are placed. The fuel rod imitator is a stainless steel pipe with copper adapter electrodes at both ends. It is centered in the glass tube by spacer grids. The glass tube is used as the outer boundary of the flow channel because it allows observation of the heat transfer processes. A SELCO ETG 602 welding power source with a maximum permanent heating input of approximately 7,500 W and short-term heating of about 15 kW is connected to the imitator electrodes.

The outlet chamber and a newly developed traverser are shown in Figure 2. The traverser contains an inbuilt set of four thermocouples designed for monitoring the temperature distribution at any location in the upper third of the HRI.

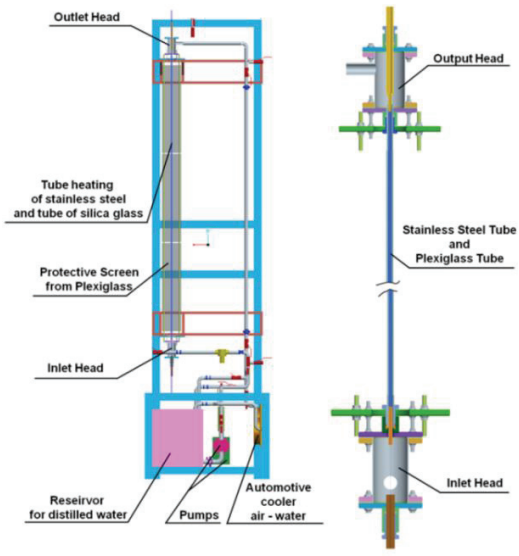

FIGURE 1. Diagram of the experimental equipment [3].

FIGURE 2. Output head with a mobile thermocouple.

DESCRIPTION OF THE CFD MODEL

Correctly designing the in-built measurement system on the experimental device to determine the origin and development of boiling was essential. The CFD simulations provided us with an initial idea of the two-phase flow along the fuel rod imitator. ANSYS FLUENT 2019 R2 software was used for all the numerical simulations in this paper. The density ratio of the liquid and vapor phase slightly exceeds 1600 due to the operating conditions on the experimental device, which has a low flow rate (with velocities from 0.2 m/s at the inlet) at atmospheric pressure. This causes convergence difficulty of the CHF simulations in most CFD codes.

TABLE 1. Nomenclature

Nomenclature		Dimension
$d_{r\text{-}in}$	Inner fuel rod imitator diameter	7 mm
$d_{r\text{-}out}$	Outer fuel rod imitator diameter	9.1 mm
$d_{g\text{-}in}$	Inner glass diameter	14.5 mm
$d_{g\text{-}out}$	Outer glass diameter	20 mm
L	Length of the test section	3000 mm
$\dot{q}_W$	Total heat flux from the wall	
$\dot{q}_C$	Convective heat flux of liquid phase	
$\dot{q}_Q$	Quenching heat flux	
$\dot{q}_E$	Evaporative heat flux	
α_l	Liquid volume fraction	
$\dot{q}_V$	Convective heat flux of vapor phase	

Geometry and Mesh

The test section consists of two main components - the heated fuel rod imitator and the glass tube surrounding it. On the experimental device, spacer grids are used to hold the HRI in its position. Their influence was not considered in the CFD simulations and will be examined in future simulations. The dimensions of individual parts are shown in Table 1. The results presented in this paper are computed using two different meshes. Since the influence of the spacer grids was neglected, the flow is presumed to be identical around the circumference. The first simulations were computed using an axisymmetric mesh with 64,000 cells. The second mesh was a 3D segment representing 1/8 of the test section, as it is possible to set a periodicity boundary condition in FLUENT software, and consisted of around one million hexahedral cells with a maximum skewness of 0.09. Both meshes are shown in Figure 1. The combination of low flow rate and significant wall temperature gradients caused problems at the heated interface. Based on this, the cell size and distribution were changed in order to stabilize these simulations.

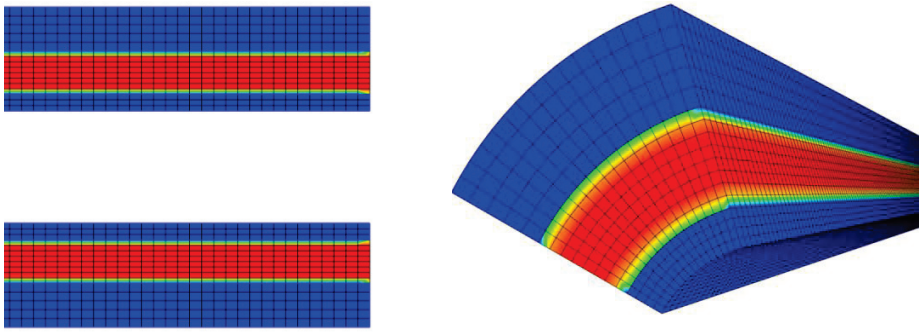

(a) (b)

FIGURE 3. (a) Axisymmetric mesh (b) Mesh of the 3D segment

CHF Model

The Eulerian multiphase model was used to allow modeling of separate, yet interacting phases. The ANSYS FLUENT solver [13] is based on the assumption that a single pressure is shared by all phases. The momentum and continuity equations are solved for each phase. The RPI model cannot be used to predict CHF because it does not include the vapor temperature in the solution process. The wall heat partition is modified as follows:

$$\dot{q}_W=(\dot{q}_C+\dot{q}_Q+\dot{q}_E)f(\alpha_l)+(1-f(\alpha_l))\dot{q}_V \quad (1)$$

An illustration of the extended RPI equation, where the heat is directly transferred from the rod to the vapor phase is shown in Figure 4.

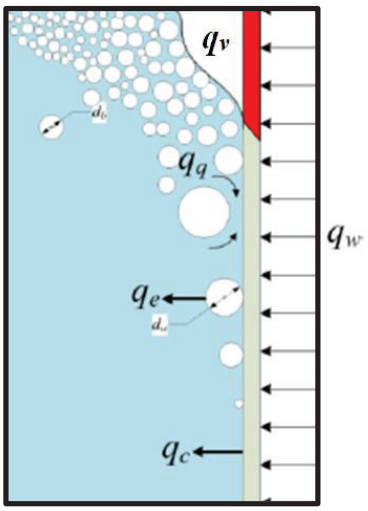

FIGURE 4. Critical heat flux model

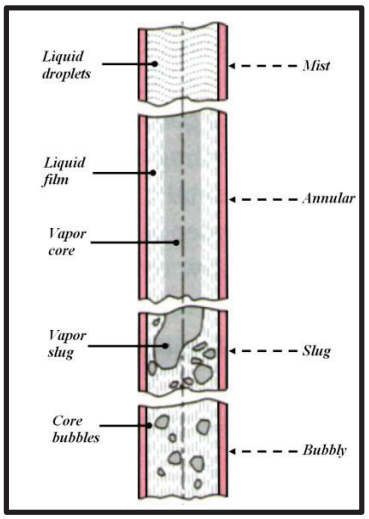

FIGURE 5. Flow regime transition visualization

The convective heat flux of the vapor phase is included as well as the liquid-phase convective heat flux, quenching heat flux and evaporation heat flux. It is computed using wall function formulations. The function $f(\alpha_l)$ depends on the local liquid volume fraction and its values lie between zero and one. After reaching the CHF and post dry-out conditions on the heated wall, where the liquid phase has been fully replaced by vapor, the multiphase flow regime changes from bubbly flow to mist flow. The flow regime transitions are shown in Figure 5. To evaluate the flow regime changes locally a cell-based interfacial surface topology is applied. This allows a smooth transition from the continuous liquid bubbly flow up to a developed mist flow. The flow regime inside each computational cell is determined depending on the vapor volume fraction, and allows the interfacial momentum transfer to be solved. Drag, lift, turbulent forces and mass exchanges are computed using various models available for each of these effects. The interfacial exchange models used are shown in Table 2.

TABLE 2. Interfacial exchange model

	Parameters	Models
Momentum transfer	Drag force	Ishii model
	Lift force	Moraga model
	Wall lubrication force	--
	Turbulent dispersion force	Lopez de Bertodano model
	Turbulent interaction force	Troshko-Hassan model
Energy transfer	Interfacial heat transfer coefficient	Ranz-Marshall model

The CHF predictions for the experimental device at the University of West Bohemia were carried out on a model with constant flow velocity at the inlet while the heating input gradually increased until the two-phase flow reached a steady state. Two different approaches under the same conditions were applied, both of which gave the same results.

The first numerical simulations were conducted using an axisymmetric model. The more advanced simulations were undertaken using a 3D segment of the tested section. With the exception of small deviations in the problematic region where the flow regime transition from annular flow and mist flow occurs, the results show good agreement. The experiments will be discussed in the results section.

THE RESULTS OF THE CFD SIMULATIONS

The simulations were performed under one constant inlet velocity and eight different wall heat fluxes at atmospheric pressure using the transient solving method. The maximum vapor volume fraction and the maximum wall temperature were monitored during the simulation to determine whether the critical heat flux occurs. The initial surface heating was set to 4300 W and gradually increased by 500 W until the CHF was detected. The main indication of the CHF occurrence was a sudden rise of temperature at the heated interface. This is shown in Figure 6 where the liquid sublayer dryout happened at the very end of the test section.

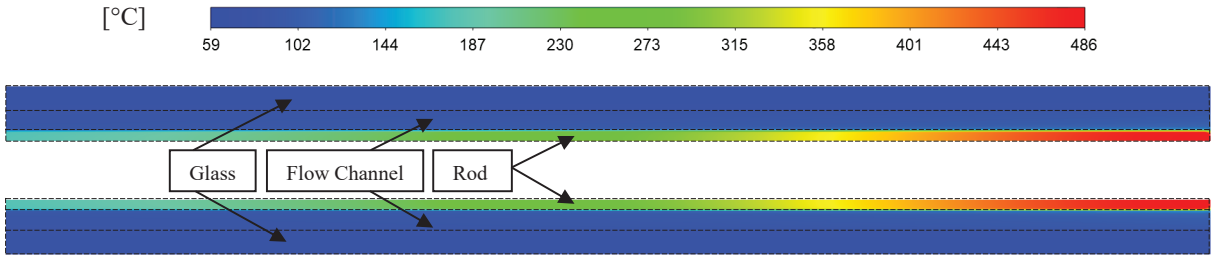

FIGURE 6. Temperature distribution along the end of the fuel rod imitator at heat transfer rate 7400 W

The goal of the simulations was to predict the minimum surface heat flux at which the CHF will occur and examine how intensely this will happen to prevent damage to the experimental device. The boundary conditions of the CFD simulations are shown in Table 3.

TABLE 3. Boundary conditions of CFD simulations

Location	Type	Value
Inlet	Velocity	0.2 m/s
	Temperature	60 °C
Turbulence	Backflow Turbulent Kinetic Energy	0.02 m^2/s^2
	Backflow Specific Dissipation Rate	1 1/s
Fuel rod imitator	Total Heat Transfer Rate	4300 W
		5000 W
		5500 W
		6000 W
		6500 W
		7000 W
		7250 W
		7400 W
Outlet	Pressure	100 kPa

There was no further increase in surface heat flux in cases where the CHF was achieved. All these computations started from the same case with the heating power 6,000 W since it was the last steady-state simulation without the liquid sublayer dryout.

The results of the preliminary CFD study are satisfactory but need to be validated on the experimental device. Vapor volume fractions along the HRI for all the considered values of the heating power are shown in Figure 7. It can be seen that the vapor volume fraction at heating inputs over 6,500 W exceeds 93 %. This further leads to a significant decrease of the heat transfer coefficient and to observing the CHF.

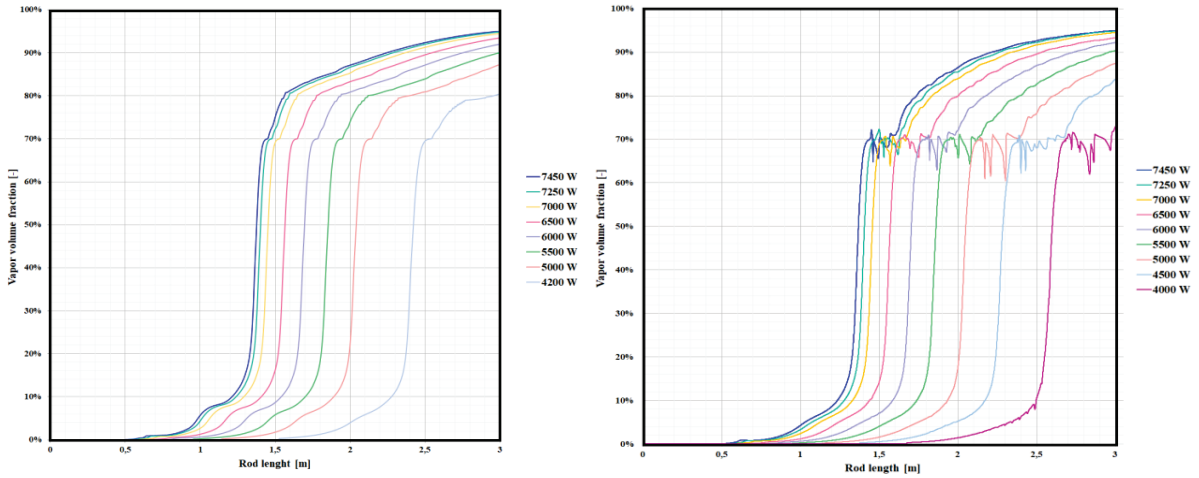

a) b)

FIGURE 7. Vapor volume fraction along the fuel rod imitator a) Axisymmetric model b) 3D segment

As mentioned above and shown in Figure 7 b) instabilities occurred during the simulations on the 3D segment in the case of transition from annular flow to mist flow. Although the vapor volume fraction in that area is locally fluctuating, the influence on the results is low. After completing the transition of the flow regimes, the flow quality starts to rise continuously and leads to overheating of the vapor phase. Both types of CFD simulations gave the same temperature distribution along the heated wall, which is shown in Figure 8.

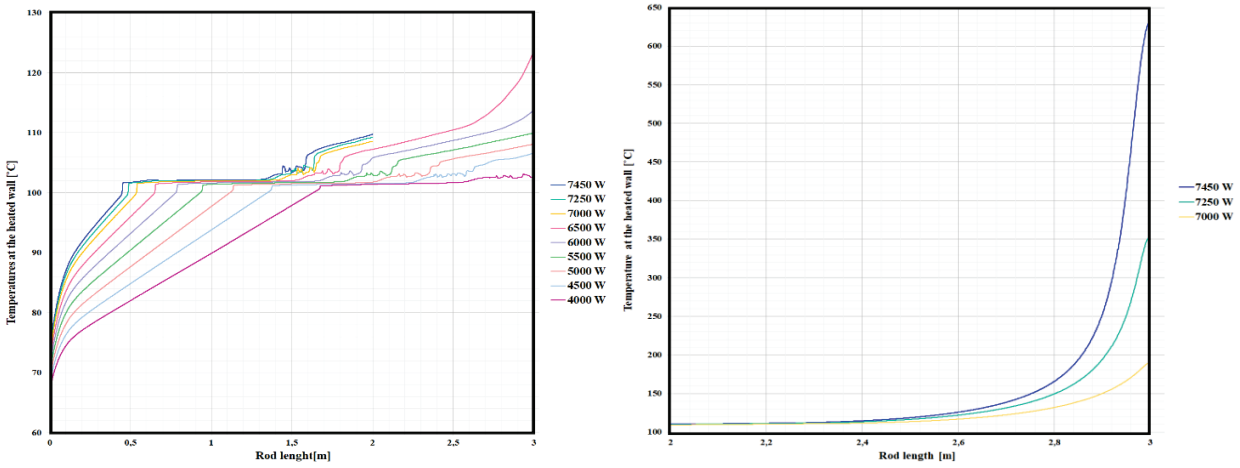

a) b)

FIGURE 8. Temperature distribution along the fuel rod imitator for a) Small or no overheating b) Significant overheating

The CHF is characterized by a low value of the heat transfer coefficient which is caused by high vapor volume fractions at the heated interface. In Figure 9 the HTC distribution along the HRI for higher values of heating power is shown. The decrease of the HTC can be well observed at heating inputs of 6,500 and 7,000 W.

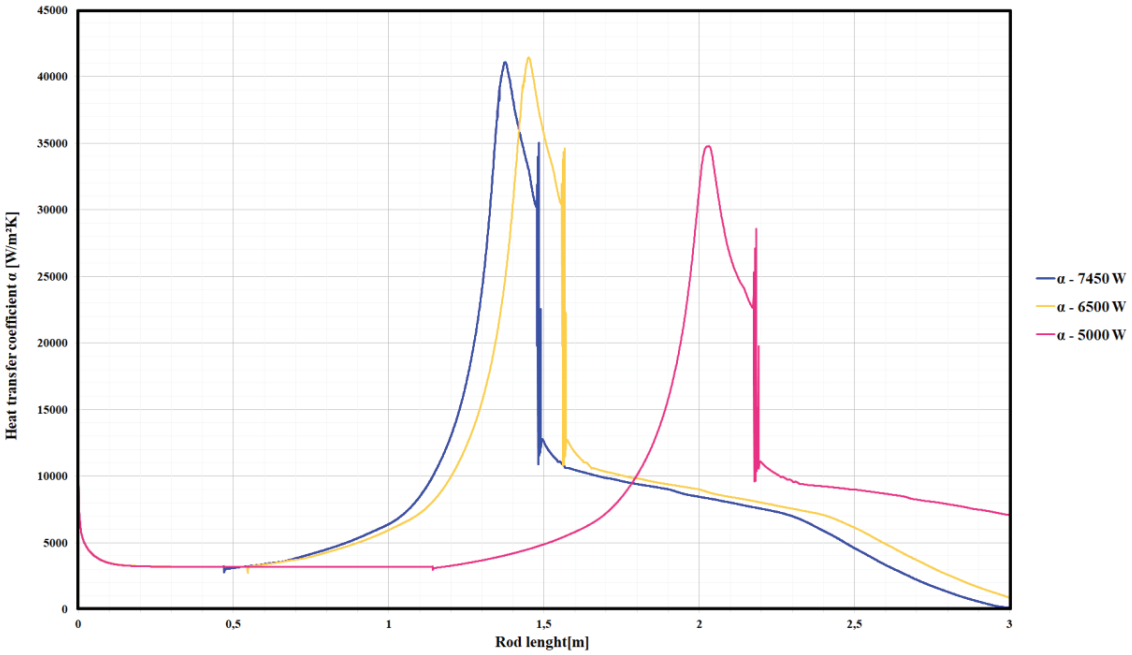

FIGURE 9. HTC distribution along the fuel rod imitator for high values of the heating power

CONCLUSIONS

In this study, a simplified CFD methodology has been used to predict liquid sublayer dryout using two different approaches. Comparison of the results shows good agreement with one another and predicts that the critical heat flux will occur in cases where the heating input exceeds 6,500 W with an inlet velocity of 0.2 m/s. The success of the tested computational methods indicates that predictions of CHF at atmospheric pressure and low flow rates can be achieved for a wide range of input parameters. The knowledge about convergence difficulties obtained from these simplified simulations allows the progress of research focused on more complex models with spacer grids and regimes at higher flow rates. Based on the simulations, some modifications to the experimental facility were designed and applied. The first test experiments were run on this modified experimental loop and validation of the CHF predictions are planned in the near future. The ultimate goal is neither to find a new approach in the measuring nor to simulate the CHF predictions, but to improve know-how and create relatively reliable, rapid and available tools for determining the CHF in collaboration with the industrial project partner which is preparing the experimental loop for measuring the real high parameters on models of real fuel rods for nuclear reactors.

ACKNOWLEDGMENTS

This paper was created as a part of the project "Experimental and computational identification of the heat transfer crisis of low power reactor fuels, SMR" TK02020033 supported by the Technology Agency of Czech Republic in the Theta program.

Furthermore, this work was financially supported by student project SGS-2019-021 (Improving the efficiency, reliability and service life of power machines and equipment 5).

REFERENCES

1. J. P. Duarte, D. Zhao, H. Jo, M. L. Corradini, “Critical heat flux experiments and a post-CHF heat transfer analysis using 2D inverse heat transfer,” in *Nucl. Eng. Des. 337,* (2018) 17–26.
2. D. Zhao, J. P. Duarte, W. Liu, M. L. Corradini, J. Wang, J. Bi, “DNB type critical heat flux prediction in rod bundles with simplified grid,“ in *Nuclear Engineering and Design 351*, (2019) pp. 94–105.
3. D. Lávička, “Od jaderného reaktoru k experimentálnímu modelu chlazení palivového proutku,“ 2010.

4. L. Suk et al, “Experimental Investigation of Critical Heat Flux on Different Surfaces at Low Pressure and Low Flow,” in *Energies 2019, xx, 5; doi:10.3390/enxx010005*
5. J.-W. Park, W.-P. Baek, S.H. Chang, “Critical heat flux and flow pattern for water flow in annular geometry,” *Nucl. Eng. Des., 172 (1997), pp. 137-155*
6. S.-Y. Chun, H.-J. Chung, S.-D. Hong, S.-K. Yang, and M.-K. Chung, “Critical Heat Flux in Uniformly Heated Vertical Annulus Under a Wide Range of Pressures 0.57–15.0 MPa,: in *J. Korean Nucl. Soc., vol. 32, no. 2, pp. 128–141, 2000.*
7. C. Haas, T. Schulenberg, T. Wetzel, “Critical heat flux for flow boiling of water at low pressure in vertical internally heated annuli,” in *Int J. Heat Mass Transf. 2013, 60, 380–391, doi:10.1016/j.ijheatmasstransfer.2012.12.038.*
8. G. Mayer, R. Nagy, I. Nagy, “An experimental study on critical heat flux in vertical annulus under low flow and low pressure conditions.” in *Nucl. Eng. Des. 2016, 310, 461–46, doi:10.1016/j.nucengdes.2016.10.026.*
9. J. Macek, L. Vyskocil, “Simulation of critical heat flux experiments in NEPTUNE_CFD code,” in *Research Article Sci. Technol. Nucl. Install., 2008* (2008)
10. L. Vyskocil, J. Macek, “CFD simulation of critical heat flux in a rod bundle,” in *Proc. CFD4NRS-3: CFD for Nuclear Reactor Safety Applications,* OECD/NEA & IAEA, Bethesda, MD, USA, 2010.
11. T. Salnikova, “Two-phase CFD analyses in fuel assembly sub-channels of pressurized water reactors under swirl conditions,” Ph.D. Thesis, Technischen Universität Dresden, Germany, 2008
12. R. Zhang, J.P. Duarte, T. Cong, M.L., “Corradini Investigation on the critical heat flux in a 2 by 2 fuel assembly under low flow rate and high pressure with a CFD methodology,” in *Ann. Nucl. Energy, 124* (2019), pp. 69-79
13. R. Zhang, T. Cong,, G. Su, J. Wang, S. Qiu, “Investigation on the critical heat flux in typical 5 by 5 rod bundle at conditions prototypical of PWR based on CFD methodology,” in *Applied Thermal Engineering Volume 179*, (2020), 115582
14. ANSYS Inc., ANSYS FLUENT Theory guide, Canonsburg, PA, USA 2019